View metadata, citation and similar papers at core.ac.uk

brought to you by CORE

provided by Elsevier - Publisher Connector

Multiple Regions of RyR1 Mediate Functional and Structural Interactions with α_{1S}-Dihydropyridine Receptors in Skeletal Muscle

Feliciano Protasi,* Cecilia Paolini,† Junichi Nakai,‡ Kurt G. Beam,§ Clara Franzini-Armstrong,† and Paul D. Allen*

*Department of Anesthesia Research, Brigham and Women's Hospital, Boston, Massachusetts 02115 USA; †Department of Cell and Developmental Biology, University of Pennsylvania, Philadelphia, Pennsylvania 19104 USA; ‡National Institute for Physiological Sciences, Okazaki 444, Japan; and §Department of Anatomy and Neurobiology, Colorado State University, Fort Collins, Colorado 80523 USA

ABSTRACT Excitation-contraction (e-c) coupling in muscle relies on the interaction between dihydropyridine receptors (DHPRs) and RyRs within Ca^{2+} release units (CRUs). In skeletal muscle this interaction is bidirectional: α_{1S}DHPRs trigger RyR1 (the skeletal form of the ryanodine receptor) to release Ca^{2+} in the absence of Ca^{2+} permeation through the DHPR, and RyR1s, in turn, affect the open probability of α_{1S}DHPRs. α_{1S}DHPR and RyR1 are linked to each other, organizing α_{1S}-DHPRs into groups of four, or tetrads. In cardiac muscle, however, α_{1C}DHPR Ca^{2+} current is important for activation of RyR2 (the cardiac isoform of the ryanodine receptor) and α_{1C}-DHPRs are not organized into tetrads. We expressed RyR1, RyR2, and four different RyR1/RyR2 chimeras (R4: Sk1635–3720, R9: Sk2659–3720, R10: Sk1635–2559, R16: Sk1837–2154) in 1B5 dyspedic myotubes to test their ability to restore skeletal-type e-c coupling and DHPR tetrads. The rank-order for restoring skeletal e-c coupling, indicated by Ca^{2+} transients in the absence of extracellular Ca^{2+}, is RyR1 > R4 > R10 ≫ R16 > R9 ≫ RyR2. The rank-order for restoration of DHPR tetrads is RyR1 > R4 = R9 > R10 = R16 ≫ RyR2. Because the skeletal segment in R9 does not overlap with that in either R10 or R16, our results indicate that multiple regions of RyR1 may interact with α_{1S}DHPRs and that the regions responsible for tetrad formation do not correspond exactly to the ones required for functional coupling.

INTRODUCTION

An increase in intracellular Ca^{2+} concentration is the signal that triggers contraction in muscle cells. A specialized intracellular store, the sarcoplasmic reticulum (SR), functions to finely control myoplasmic [Ca^{2+}] in response to depolarization of the plasmalemma. The series of events that allows the transduction of the sarcolemma depolarization into Ca^{2+} release is called excitation-contraction (e-c) coupling. The two membrane systems, plasmalemma and SR, communicate very efficiently with each other at specific structures called calcium release units (CRUs) or junctions. These structures contain proteins that have been identified as key elements in the process: the ryanodine receptors (RyRs), large intracellular channels (~2260 kDa) that allow Ca^{2+} to exit the SR in response to depolarization of the plasma membrane (for reviews see Coronado et al., 1994; Meissner, 1994; Sutko and Airey, 1996; Franzini-Armstrong and Protasi, 1997) and the dihydropyridine receptors (DHPRs), L-type voltage-gated Ca^{2+} channels that are present in the exterior membranes of muscle cells and that control the opening of RyRs (Fosset et al., 1983; Pincon-Raymond et al., 1985; Rios and Brum, 1987; Tanabe et al., 1987, 1988).

While DHPRs and RyRs are the two proteins primarily responsible for transduction of the electrical signal in both cardiac and skeletal muscle cells, it has become increasingly evident that the way in which they communicate with each other is different in the two muscle types. In both types of muscle, depolarization of the plasma membrane activates the voltage-gated DHPRs, thereby allowing Ca^{2+} to enter the cells from the extracellular space. In cardiac muscle, this Ca^{2+} influx through the α_{1C}(α_1 cardiac)DHPR is the principal signal that induces the opening of RyR2 and the consequent massive release of Ca^{2+} into the myoplasm (calcium induced calcium release, CICR; Fabiato, 1983, 1985). In fact, e-c coupling in cardiac muscle fails in the absence of extracellular Ca^{2+}. In skeletal muscle, however, Ca^{2+} entry is not required for the communication between α_{1S}(α_1 skeletal)DHPR and RyR1, and e-c coupling continues in the absence of extracellular Ca^{2+} (Rios et al., 1991; Schneider, 1994). To elucidate the e-c coupling mechanism in skeletal muscle cells it is essential to understand how RyRs and DHPRs communicate with each other without the need for Ca^{2+} as a messenger. Electron microscopy studies reveal that RyR1 and α_{1S}DHPR have a highly specific association that results in the formation of tetrads, groups of four DHPRs linked to subunits of alternate RyRs (Block et al., 1988; Franzini-Armstrong and Kish, 1995; Protasi et al., 1997). Taken together, the structural and functional observations point to a mechanical coupling of RyR1/α_{1S}DHPR similar to the mechanism first suggested by Schneider and Chandler (1973). The DHPR functions as a voltage sensor that changes its conformation in response to depolarization, and this change in conformation then triggers RyR opening

Submitted March 22, 2002, and accepted for publication July 31, 2002.

Address reprint requests to Dr. Cecilia Paolini, Department of Cell and Developmental Biology, University of Pennsylvania, School of Medicine, B1 Anatomy Chemistry Bldg., Philadelphia, PA 02115. Tel.: 215-898-3345; Fax: 215-573-2170; E-mail: cpaolini@mail.med.upenn.edu.

© 2002 by the Biophysical Society

0006-3495/02/12/3230/15 $2.00

directly without the need of a diffusible messenger (orthograde signaling). RyR1, in turn, affects gating properties of the DHPR (Nakai et al., 1996; Avila and Dirksen, 2000), with the result that the amplitude of the L-type Ca^{2+} current is increased (retrograde signaling).

Two animal models have been extremely valuable tools in dissecting skeletal e-c coupling: the *dysgenic mouse* (mdg), having a spontaneous mutation in the α_{1S}DHPR gene that eliminates slowly activating Ca^{2+} current and intramembrane charge movement (Beam et al., 1986; Adams et al., 1990; Chaudhari, 1992), and the *dyspedic mouse*, having a targeted null mutation of RyR1 (Takeshima et al., 1994; Buck et al., 1997). In both cases e-c coupling fails, but can be restored by transfection of the myotubes with cDNA encoding the missing protein (Tanabe et al., 1988; Nakai et al., 1996; Moore et al., 1998), thus directly proving the primary roles of α_{1S}DHPR and RyR1 in e-c coupling. The identification of key domains of α_{1S}DHPR that allow communication with RyR1 has come from the use of skeletal-cardiac and, more recently, skeletal-insect chimeras. In these chimeric DHPRs the II-III loop of the skeletal DHPR, or even a shorter subdomain of it (containing only 46 amino acids), is sufficient to restore skeletal-type e-c coupling and retrograde signaling (Tanabe et al., 1990; Nakai et al., 1998b; Grabner et al., 1999). Even drastic alteration of the sequence surrounding those 46 amino acids does not abolish the ability to support skeletal type e-c coupling or retrograde signaling (Wilkens et al., 2001). For the RyR, an analogous approach has been taken of constructing chimeras in which portions of RyR2 (the cardiac RyR isoform) are replaced with the corresponding segments of RyR1. Expression of such chimeras in dyspedic myotubes shows that both skeletal-type e-c coupling and retrograde signaling are strongly restored by the chimera R10, which contains skeletal residues 1635–2559, whereas only retrograde coupling is strong for the chimera R9, which contains skeletal residues 2659–3720 (Nakai et al., 1998a). Subsequently, it has been shown that the chimera R16, which contains RyR1 residues 1837–2154, mediates weak skeletal-type coupling (Proenza et al., 2002).

Continuing the search for the molecular and structural basis for RyR1/α_{1S}DHPR interactions, we have expressed RyR1, RyR2, and four different RyR1/RyR2 chimeras (R9, R10, R16, and also R4, which contains skeletal residues 1635–3720) in 1B5 cells (a mouse skeletal muscle cell line that carries a null mutation for RyR1) and tested for a correlation between the presence of tetrads and Ca^{2+}-entry independent e-c coupling. Differentiated 1B5 cells develop a SR system that forms junctions with the surface membrane and with primitive transverse (T)-tubules despite the lack of RyRs (Protasi et al., 1998). These junctions contain triadin and DHPRs, but of course lack RyRs, or feet (dyspedic CRUs), and thus do not support Ca^{2+} release in response to depolarization, caffeine or 4-m-chloro-cresol (Moore et al., 1998; Fessenden et al., 2000). Dyspedic CRUs (dCRUs) in 1B5 cells resemble junctions in developing myotubes of RyR1-null mice (Takeshima et al., 1994; Takekura et al., 1995; Takekura and Franzini-Armstrong, 1999). In the absence of RyRs, DHPRs do not maintain the normal tetradic arrangement that is found in wild-type skeletal muscle cells (Protasi et al., 1998). Arrays of DHPR tetrads and skeletal-type e-c coupling can be restored in differentiated 1B5 cells by transfection with RyR1 cDNA (Fessenden et al., 2000; Protasi et al., 2000). Our results with chimeric RyRs show that the presence of at least two non-overlapping regions of RyR1 primary sequence are sufficient to restore tetrads and skeletal-type e-c coupling, although with a somewhat variable degree of success, suggesting multiple sites of interaction between RyR1 and the DHPR. Interestingly, the RyR1 sites responsible for functional coupling with the DHPR only partially correlate with those that allow the structural linkage between the two proteins.

MATERIALS AND METHODS

Cell culturing

The methods used to create the 1B5 cell line are described in detail elsewhere (Moore et al., 1998). The cells were expanded at 37°C in low-glucose DME medium containing 20% fetal bovine serum, 100 U/ml penicillin, 100 μg/ml streptomycin, and an additional 2 mM L-glutamine (growth medium). After ~48 h the cells were re-plated in either 1) 35-mm dishes containing thermanox coverslips for electron microscopy and immunocytochemistry (Nunc Inc., Naperville, IL); or 2) in 96-well plates with ultra-thin, clear bottoms for Ca^{2+} imaging experiments (Corning Incorporated, Costar, NY) coated with Matrigel (Collaborative Biomedical Products, Bedford, MA). When cells reached ~70% confluence, growth medium was replaced with differentiation medium (growth medium with 5% heat-inactivated horse serum replacing the 20% fetal bovine serum) to induce differentiation. The medium was changed daily.

cDNA packaging in HSV-1 virions and cell transfection

The cDNAs encoding for RyR1, RyR2, and the four RyR1/RyR2 chimeras were packaged into HSV-1 amplicon virions using the helper virus-free packaging system. The methods are described in detail elsewhere (Fraefel et al., 1996; Wang et al., 2000). Four to five days after the beginning of differentiation, the cells were infected with 1 ml differentiation medium containing HSV1 virions at 4×10^5 infectious units/ml (a moiety of infection of ~4). This mixture was removed ~2 h later and replaced with differentiation medium. The cells were either fixed or imaged ~24–36 h later.

Immunohistochemistry

The cells were fixed in methanol for a minimum of 20 min at −20°C, blocked in PBS (phosphate-buffered saline: 26.7 mM Na_2HPO_4, 7.3 mM KH_2PO_4, 136.8 mM NaCl, 2.6 mM KCl) containing 1% BSA and 10% goat serum for 1 h, incubated first with primary antibodies and then with secondary antibodies (cyanine 3 conjugated; Jackson ImmunoResearch Laboratories, Lexington, KY), respectively, for 2 h and 1 h at room temperature. Code, specificity, working dilution, original reference, and the sources of primary antibodies are as follows: 34C, recognizes RyR1, R4,

and R9, 1:20, Airey et al., 1990, Developmental Studies Hybridoma Bank, The University of Iowa; C3-33 recognizes RyR2, R10, and R16, 1:20, gift of G. Meissner (Junker et al., 1994). The specimens were viewed on an inverted fluorescence microscope (Olympus IX70).

Electron microscopy

The cells were washed twice in PBS at 37°C, fixed in 3.5% glutaraldehyde in 0.1 M sodium cacodylate buffer, pH 7.2, and then kept in fixative for up to one to four weeks at 4°C before further use. For thin-sectioning the cells were post-fixed in 2% OsO_4 for 2 h at room temperature and then contrasted in saturated uranyl acetate either for 4 h at 60°C or overnight at room temperature. The samples were embedded in Epon 812, and the sections stained in uranyl acetate and lead for ~8 min each. For freeze-fractures the glutaraldehyde-fixed cells were infiltrated with 30% glycerol. A small piece of the coverslip was mounted with the cells facing a droplet of 30% glycerol, 20% polyvinyl alcohol on a gold holder, and then frozen in liquid nitrogen-cooled propane (Cohen and Pumplin, 1979; Osame et al., 1981). The coverslip was flipped off to produce a fracture that followed the culture surface originally facing the coverslip. The fractured surfaces were shadowed with platinum unidirectionally at 45° and then replicated with carbon in a freeze-fracture apparatus (Balzers, model BFA 400; Balzers S.p.A., Milan, Italy). Sections and replicas were photographed in a 410 Electron Microscope (Philips Electron Optics, Mahwah, NJ).

Ca^{2+} imaging

Twenty-four to thirty-six hours after transduction, cells were loaded with the Ca^{2+} fluorescent dye, Fluo-4 AM (Molecular Probes, Eugene, OR) to monitor intracellular changes in $[Ca^{2+}]$. The loading procedure was 1) differentiation media was removed and cells were washed twice with imaging buffer (IB) containing 125 mM NaCl, 5 mM KCl, 1.2 mM $MgSO_4$, 6 mM glucose, 25 mM HEPES, 0.05% BSA, 2 mM $CaCl_2$, pH 7.4; 2) the cells were incubated for 30 min in 100 μl IB containing 5 μM Fluo-4 AM; 3) cells were washed again with IB. The 96-well plates, containing a monolayer of 1B5 cells transduced with one of the RyR constructs, were placed on the stage of a Nikon Diaphot 300 inverted microscope equipped with an Olympus Uapo/340 40× oil immersion objective (numerical aperture 1.35) for study at room temperature (~21°C). The microscope was modified to incorporate a pair of separate 3-D micromanipulators on either side of the vertical post holding the condenser. Each well in the 96-well plate could be perfused in a controllable, accurate way using an AutoMate 8-channel air pressure-controlled system incorporating multiple 50-ml reservoirs (Automate Scientific Inc., Berkeley, CA). Each reservoir could be rapidly switched into or out of the perfusion pathway with a ~50 μl dead volume. The 3-D micromanipulators were used to place a pair of capillaries precisely into each well: 1) an inlet to allow delivery of the desired medium, and 2) a vacuum suction outlet to keep the level of medium in the well constant. The perfusion inlet was positioned ~1 mm above the imaged cell/myotube to allow a very efficient and rapid change of solution over the imaged area. Before starting the experiments IB was replaced in all Fluo-4 AM-loaded wells with nominally Ca^{2+}-free IB, in which the $CaCl_2$ was replaced with 0.5 mM $CdCl_2$ and 0.1 mM $LaCl_3$ to block Ca^{2+} currents through DHPRs. Four regions with a size of ~½ of the cell diameter were selected in four different myotubes. The selected regions were from apparently well-differentiated (large) myotubes and contained no nuclei. The cells were imaged using a PTI delta-RAM as the light source with a Stanford Photonics 12-bit digital intensified CCD and the data displayed and analyzed using QED imaging software (v1.3. QED Software, Pittsburgh, PA). The four areas were simultaneously recorded using the strip chart utility in the QED software to monitor image intensity. In each well, the cells were first perfused for at least 1 min with Ca^{2+}-free IB and then stimulated by separate 15-s exposures to Ca^{2+}-free 80 mM K^+ and 40 mM caffeine, with a 15-s recovery period in between. The Ca^{2+}-free 80 mM K^+ consisted of Ca^{2+}-free IB, which had equimolar substitution of 80 mM K^+ for Na^+. The resulting fluorescence changes were corrected for background by subtraction of the average fluorescence value in the 5 s preceding the test stimulus. Two measures were used to estimate the ability of each of the RyR constructs to restore skeletal-type e-c coupling. The first was to determine the number of cells producing a Ca^{2+} transient in response to K^+ depolarization relative to the number of cells producing a Ca^{2+} transient in response to caffeine. The second was to determine the ratio of the magnitudes of the responses to K^+ depolarization and caffeine, respectively.

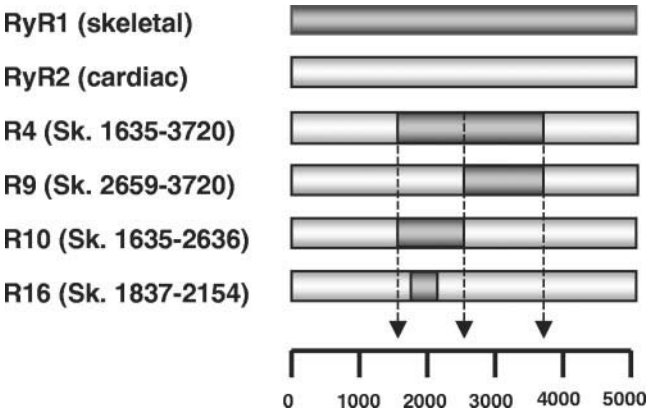

FIGURE 1 Schematic representation of RyR chimeras. Skeletal sequence (from RyR1) is represented in dark gray; cardiac sequence (from RyR2) is represented in lighter gray. Amino acid composition of the chimeras R4, R9, and R10 are as in Nakai et al., 1998a. R4: Ca(1–1625), Sk(1635–3720), Ca(3687–4968); R9: Ca(1–2624), Sk(2659–3720), Ca(3687–4968); R10: Ca(1–1625), Sk(1635–2636), Ca(2603–4968). Amino acid composition of R16 is as in Proenza et al., 2002: Ca(1–1817), Sk(1837–2154), Ca(2118–4968).

Preparation of figures

Pictures and negatives were scanned using a Color Flatbed Scanner UMAX Power Look II at 300 dpi. Figures were mounted and labeled using Adobe Photoshop v5.5, Canvas v3.5.4 (Deneba Software), and Microsoft Power Point 98.

RESULTS

Immunocytochemistry

Differentiating 1B5 cells have been previously described in detail (Protasi et al., 1998). Of relevance to this work is the relationship between the formation of large multinucleated myotubes and the presence of dCRUs (dyspedic peripheral couplings, dyads, and triads) containing co-localized DHPRs and triadin foci (Protasi et al., 1998, 2000).

Infection of 1B5 cells with HSV-1 amplicon virions containing cDNA encoding any of the six constructs tested in this work (Fig. 1) results in a large fraction of all cells expressing protein at a substantial level. Fig. 2 illustrates low-magnification images of myotubes immunostained with anti-RyR antibodies (either 34C or C3-33) 24–36 h after

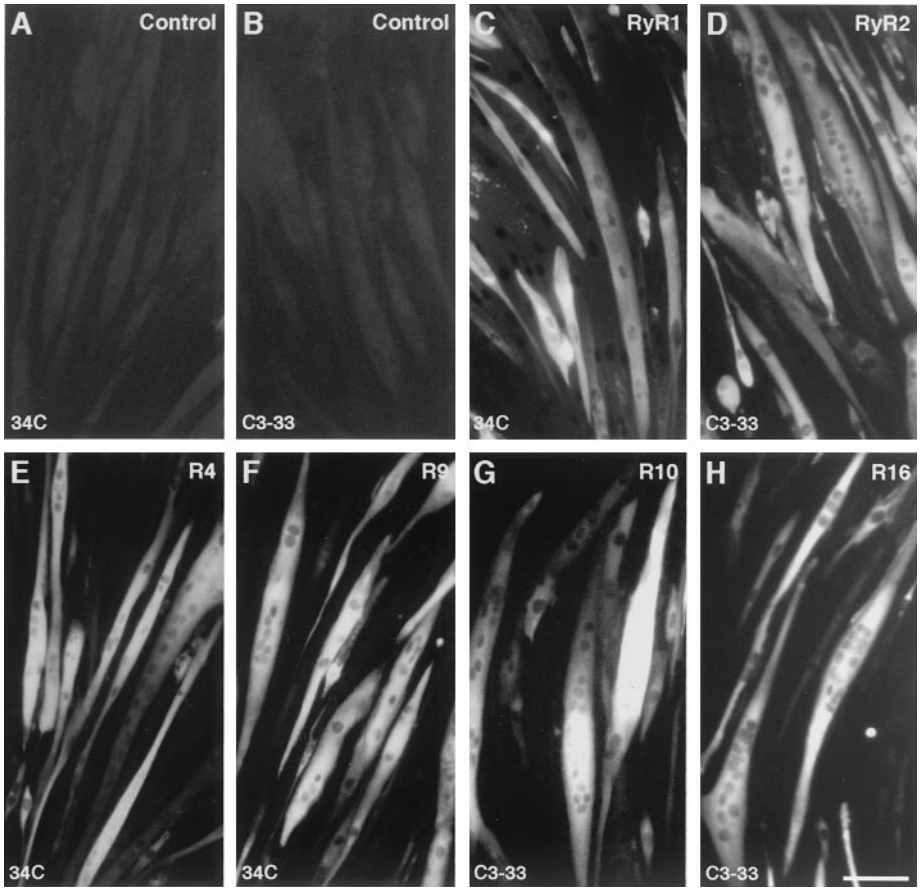

FIGURE 2 HSV1 virions give transfection of high efficiency. (*A* and *B*) Lack of labeling of control cells with 34C and C3-33, the two antibodies used to detect RyR1, RyR2 and the four chimeric RyRs. (*C–H*) Immunostaining of transduced cells shows that a high percentage of myotubes react positively to anti-RyR antibodies. Functional studies confirm that ~80% of the cells respond functionally to caffeine (Fig. 8, Table 2). Bar: 200 μm.

infection. The number of cells stained with anti-RyR antibodies agrees with functional results showing that ~80% of the cells respond to caffeine in each sample group (see Ca^{2+} imaging section, Fig. 8, and Table 2 for more details). Infection with HSV-1 amplicon virions does not appear to cause any cell death, obvious changes in cell size and shape, or the level of differentiation. High-magnification immunofluorescence images reveal that all RyRs expressed in our cells were clustered in intense foci (Fig. 3). Focusing up and down clearly shows that the majority of these immunopositive foci are located at, or very near, the surface membrane, on both ventral and dorsal sides of the myotubes. The cortical localization of these positive foci coincides with that previously shown for CRUs in both RyR1-containing and RyR1-lacking myotubes (Protasi et al., 1998, 2000). Control 1B5 myotubes (non-transduced) do not react with either one of the antibodies (34C against RyR1 and RyR3 and C3-33 against RyR2) used to detect RyR expression in transduced myotubes (Fig. 2, *A* and *B*, Fig. 3, *A* and *B*), confirming that these cells do not express detectable levels of any RyR.

Electron microscopy

Thin sections

In thin-section electron microscopy, differentiated 1B5 cells are identifiable by the presence of dyspedic (dCRUs), peripherally located junctions between the SR and exterior membrane (Fig. 4 *A*). Transduction of the 1B5 cells with HSV-1 virions containing cDNA for RyR1, RyR2, or the four RyR chimeras lead to the presence of feet within the junctional gap of CRUs (*arrows* in Fig. 4, *B–G*). For all the constructs, clusters of feet are found within CRUs located at, or very near, the surface membrane and are almost never seen in the central core of the cell. This arrangement is in agreement with the peripheral location of RyR foci detected by immunolabeling (Fig. 3, see also Fig. 3 in Protasi et al., 1998) and indicates that the constructs are appropriately targeted and inserted at CRUs. However, there are distinctions between the clusters of feet produced by the different constructs. RyR2, while correctly targeted to SR-surface membrane junctions (Fig. 4 *C*, *arrows*), usually make small arrays when compared to RyR1 (Fig. 4 *B*). Due to the small

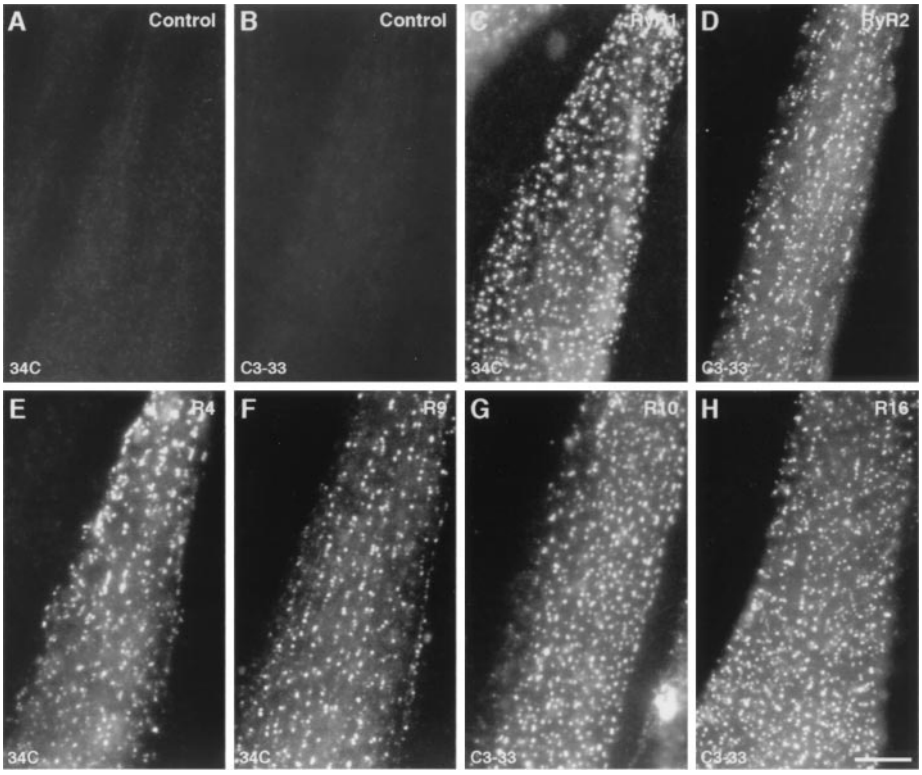

FIGURE 3 RyRs are clustered in foci. (*A* and *B*) Untreated cultures show no labeling with either 34C or C3-33 antibodies. (*C–H*) All RyRs expressed in 1B5 cells cluster within intensely labeled foci located at the periphery of large and differentiated myotubes. The images are not confocal, but were taken with a high numerical aperture objective. The focal plane in all cases is at or close to the lower, flat surface of the cell. There are no obvious differences between the various constructs. Clustering in foci is consistent with the correct targeting of all proteins to CRUs, as confirmed by thin sectioning (see Fig. 4). Bar: 25 μm.

number of feet visible in each sectioned CRU (usually two to three) it is not possible to tell whether the spacing between them is regular. The RyR2 clusters in these cells are smaller than clusters in cardiac muscle junctions (Franzini-Armstrong et al., 1999), but are consistent with the small groups of feet seen in primary dyspedic cultures transfected with RyR2 (Nakai et al., 1997). Among the chimeras, R4 and R9 definitely make arrays containing several feet in ordered disposition (Fig. 4, *D* and *E*), similar to those seen with RyR1. However, the arrays of feet for R10 and R16 are not only smaller, but also apparently less ordered. In fact, in the latter two samples individual feet have a variable appearance, as if the molecules were being viewed at different angles (Fig. 4, *F* and *G*).

Freeze-fracture

In the following structural analysis of freeze-fracture replicas, we describe the effect of expressing RyR1, RyR2, and various RyR1/RyR2 chimeras on the arrangement of DHPR clusters, with the aim of identifying regions of RyR1 that may interact structurally with α_{1S}DHPRs. Untreated 1B5 cells were used as a control to show the disposition of DHPRs in the absence of interaction with RyRs. As previously shown, dyspedic 1B5 cells display clusters of DHPRs that are localized in correspondence of CRUs, as revealed by immunostaining experiments (Protasi et al., 1998). Using freeze-fracture, we identify DHPR clusters based on the large and uniform size of the particles within the cluster, as already shown in a variety of cells and configurations (Franzini-Armstrong, 1984; Block et al., 1988; Franzini-Armstrong and Kish, 1995; Takekura et al., 1995; Protasi et al., 1997, 1998, 2000). Examination of DHPR clusters in control 1B5 cells (Fig. 5 *A*) shows that particles representing DHPRs are randomly scattered within the clusters and rarely grouped in a tetrad-like configuration (see also Protasi et al., 1998). In addition, there is no alignment of particles along orthogonal directions. Such alignment indicates the presence of a stereospecific α_{1S}DHPR-RyR1 link. The lack of DHPR-tetradic arrangement in control 1B5 cells has been traced to a lack of RyR1 in the SR membrane, since tetrads are restored by RyR1 expression. RyR1-restored tetrads have a spacing and disposition identical to that of tetrads in native muscle, and thus they result from the association of groups of four DHPRs with alternate feet arranged in an orthogonal disposition (Fig. 5 *B*; see also Protasi et al., 1998, 2000). Tetrads may be incomplete; that is, one or more particles may be missing from the corners of

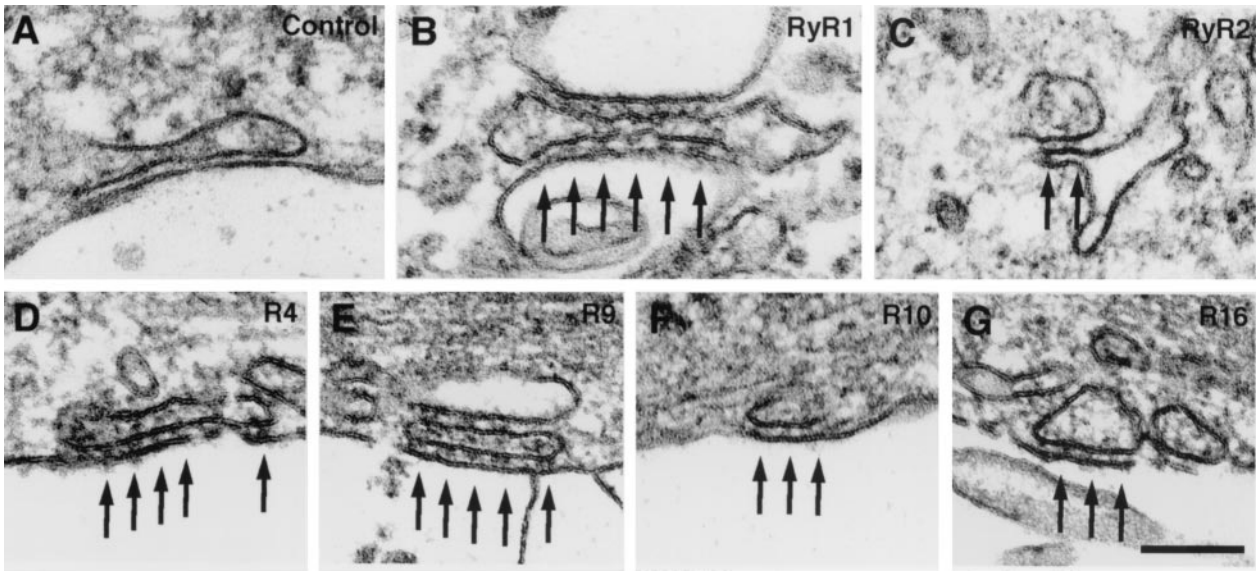

FIGURE 4 RyRs are targeted to junctions between SR terminal cisternae and the exterior membrane. (*A*) Control 1B5 cells have dyspedic junctions, i.e., no feet are visible in the junctional gap between the two membranes. (*B*) RyR1 is clustered in fairly extensive and ordered arrays (*arrows*). (*C*) RyR2 is usually present within small junctions and makes smaller clusters (*arrow*, compare with RyR1). (*D* and *E*) R4 and R9 make fairly extensive and ordered arrays, similarly to RyR1 (*arrows*). (*F* and *G*) R10 and R16 are present within the junctional gap, but the individual feet are not as clearly visible (*arrows*). This may be due to variable orientation and/or disordered array (see Fig. 7 *B*), resulting in poor overlap of the two layers of feet that are included in a thin section of standard thickness (50–60 nm). Bar: 0.1 μm.

each square. Tetrads in RyR1-expressing cells are clustered over regions of the membrane, which have a small convexity, presumably due to the presence of SR bearing feet right under the membrane. The SR domains have variable size, and contain RyR groups with variable numbers of feet.

RyR2-infected cells do not show tetrads, so the presence of tetrads cannot be used to identify cells expressing this protein and/or DHPR/RyR association. Having looked at a total of 57 well-differentiated cells showing DHPR clusters, in cultures with at least 50% infection efficiency (usually much more), we are sure that cells expressing RyR2 are included in this sample. In some of these cells, DHPRs are clustered into small groups (Fig. 5 *C*), presumably, as above, associated with feet. The small size of these sites is in keeping with the small groups of feet in RyR2-expressing cells (Fig. 4 *C*). Within the clusters the DHPR particles are randomly arranged, but rare 3-particle tetrad-like arrangements were found (Fig. 5 *C*, see box).

Differently from RyR2, the R4 chimera, which contains a large segment of RyR1 (1635–3720), are quite effective in tetrad restoration (Fig. 5 *D*). Fig. 5, *D* and *E* show two copies of the same R4-induced tetrad array: the centers of tetrads are dotted in *E*, showing that the great majority of particles in the array cluster around the dots. Dots define a very ordered tetragonal arrangement, and the center-to-center spacing between dots in the direction of the two dashed lines is ~40 nm. Tetrad disposition and spacings in R4-expressing cells mimic exactly those of native skeletal muscle (Block et al., 1988; Takekura et al., 1995; Franzini-Armstrong and Kish, 1995) and of RyR1-transfected 1B5 cells (Fig. 5 *B* and Protasi et al., 2000). In some cells expressing R4 the particles fit around the tetragonal arrangement of dots only over limited distances and then shift to a new alignment (not shown). In others, the arrays of tetrads due to R4 are sometimes small, due to clustering of RyRs in small groups. Details of tetrads and a smaller tetrad array are shown. The center-to-center distance between the particles of a tetrad is 16–18 nm, also in keeping with tetrad size in native skeletal muscle (Franzini-Armstrong and Kish, 1995).

In skeletal muscle, DHPR tetrads form because of a stereospecific α_{1S}DHPR-RyR1 association, and the disposition of dots marking the center of tetrads can be used to deduct the disposition of underlying feet. The disposition of tetrads in R4-expressing cells (Fig. 5 *E*) is consistent with ordered arrays of feet identical to those formed by RyR1 in native skeletal muscle (Ferguson et al., 1984; Block et al., 1988) and with the association of tetrads with alternate feet as described for wild-type and RyR1-reconstituted CRUs (Block et al., 1988; Franzini-Armstrong and Kish, 1995; Protasi et al., 1997, 2000). The number of particles at each position, however, varies between 1 and 4, indicating that the complement of DHPRs in the tetrads is not always complete. As discussed in detail in Protasi et al. (1997), tetrads may appear incomplete either because they actually miss one or more components or because one of the components breaks during fracturing. In the incomplete tetrads of these cells we mostly see empty positions rather than

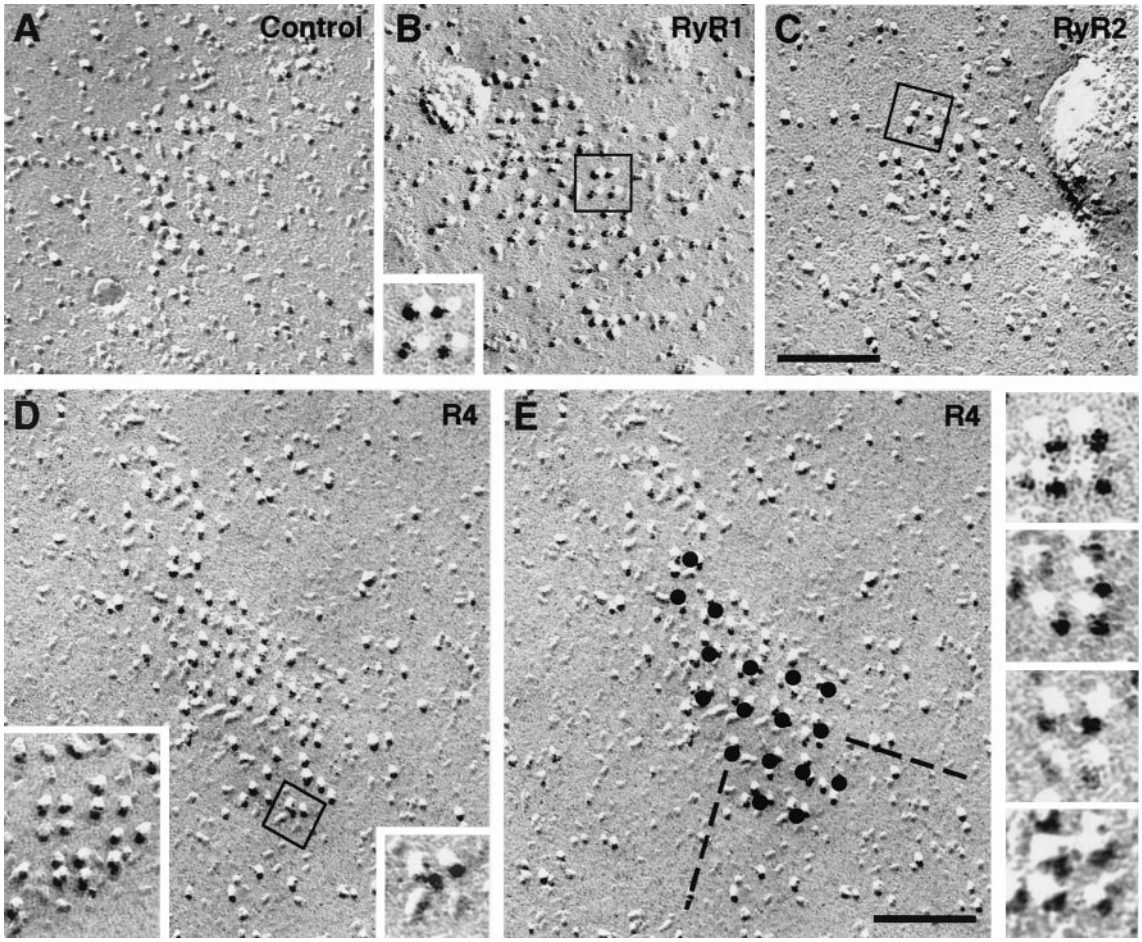

FIGURE 5 RyR1 and R4 restore extensive DHPR junctional tetrads in surface membranes of 1B5 myotubes. (*A*) In control 1B5 cells, DHPRs are clustered within junctional domains but they do not form tetrads (see Protasi et al., 1998). (*B*) RyR1 expression restores DHPR tetrads and tetrad arrays, even though some tetrads are incomplete (see Protasi et al., 2000 for further details). The boxed tetrad is shown at higher magnification in the inset. (*C*) RyR2 expression does not restore complete DHPR-tetrads, but occasional groups of three tetrad-like particles (*boxed*) are seen. (*D*) Expression of R4, the chimera containing the skeletal segment 1635–3720, restores DHPR tetrads even though some of them are incomplete. The boxed tetrad is shown at higher magnification in the inset, and well-defined tetrads from other R4-expressing cells are shown in the inset at the lower left and far right of panel *E*. (*E*) Dotting the center of each tetrad in the same array as shown in panel *D* makes it evident that the tetrads are arrayed in an ordered orthogonal arrangement. The spacing between the dots marking the center of tetrads is consistent with tetrads being superimposed on alternate RyRs, indicating that the normal skeletal 2:1 ratio between feet and tetrads is restored. Bars: 0.1 μm.

broken stumps, and thus we assume that the particles are actually missing.

The expression of R9 restores arrays of organized DHPR tetrads (Fig. 6, *A* and *B* and details of tetrads below) with parameters equal to RyR1- and R4-induced arrays. As shown by the dots in Fig. 6 *B*, the orthogonal arrangement of DHPR tetrads often extend over a relatively large area in R9-expressing cells, in agreement with the well-defined rows of feet seen in thin sections of R9-rescued CRUs (Fig. 4 *E*). Thus, in R9- and R4-expressing myotubes, feet are arranged in an ordered array and the normal skeletal ratio of 2:1 between feet and tetrads is restored.

R10 and R16 also restore tetrads, but the tetrads appear to be less frequent, less complete, and the arrays to be less ordered. In most cases it is not possible to define the disposition of tetrads for R10 and R16 because of their variable orientations and spacings. In those areas where some order is present (as in the examples of Fig. 6, *C–D*, and *F–G*), the dotted centers of tetrads are aligned over a limited distance. The probable cause for the disorder within clusters of R10- and R16-induced tetrads is that R10 and R16 may have a poor neighbor-neighbor interaction that results in a disordered disposition of feet in the SR. Thin-section images in fact, confirm this possibility (Fig. 4, *F* and *G*). Thus, each cluster of DHPRs associated to R10 and R16 would contain complete and incomplete tetrads with a more variable orientation than tetrads associated with RyR1, R4, or R9. Under these circumstances, tetrads composed of 4 or 3 particles would be detectable, but 1 or 2 DHPRs associ-

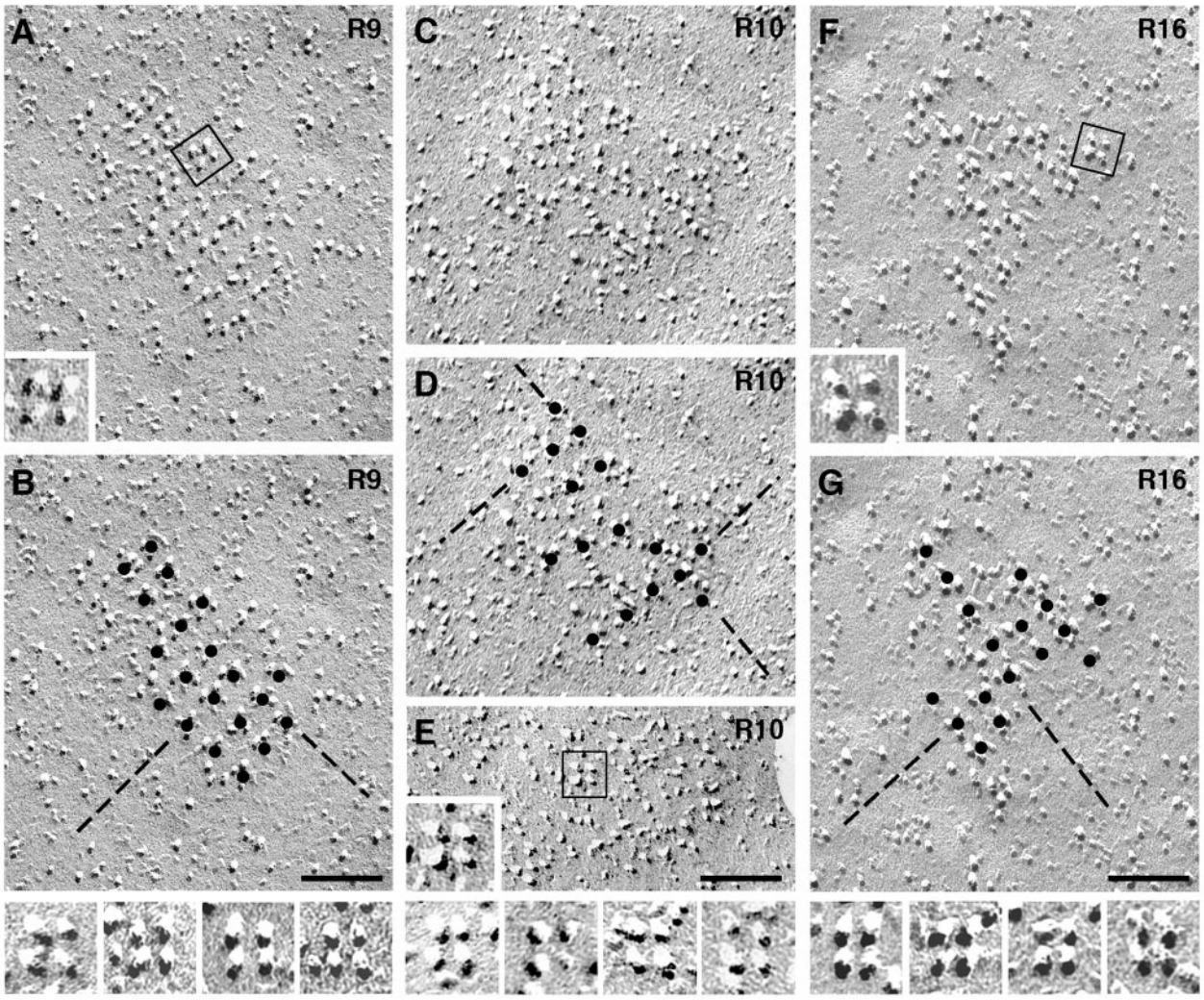

FIGURE 6 R9, R10, and R16 restore junctional tetrads and, to some extent, tetrad arrays. (*A* and *B*) An array of DHPR tetrads in an R9-expressing cell: dots marking the center of complete and incomplete tetrads form an orthogonal arrangement much like tetrad arrays in normal skeletal muscle cells and in 1B5 myotubes expressing R4 (see Fig. 5, *D* and *E*) or RyR1 (Protasi et al., 2000). Higher-magnification images are shown for the boxed tetrad in *A* (*inset*) and for four tetrads from other R9-expressing cells are below panel *B*. (*C*, *D* and *F*, *G*) Clusters of tetrads in cells expressing R10 and R16, respectively. As shown by the dots, the tetrads form orthogonal arrays in which the order extends for only a limited distance. The examples shown here are among the most ordered clusters found for R10 and R16. (*E*) A cluster of DHPRs in another R10-expressing cell. Higher magnification views of the tetrads outlined by squares are shown in the insets in *E* and *F*, and additional higher-magnification views of selected tetrads from R10- and R16-expressing cells are shown below *E* and *F*, respectively. The presence of only short-range order in the tetrad arrays for R10 and R16 is probably due to the fact that these two chimeras fail to assemble into ordered arrays of feet in the SR membrane (see Figs. 4 and 7 for comparison). Bars: 0.1 μm.

ated with a foot would not be detectable, even if the association is stereospecific.

To better define the variable occupancy of feet by DHPRs described above, we have quantified tetrad frequencies within defined DHPR clusters. The first aim is to find out how effectively each chimera formed tetrads rather than to estimate how frequent tetrads are in each cell. For that reason, we specifically selected clusters that appeared most populated by tetrads (or tetrad-like structures) in each sample. The data were obtained by counting the number of particles located either at the four corners of a small square (4-particle tetrads), or at three corners of a square (incomplete, or 3-particle tetrads). Groups of particles were counted as tetrad-like configurations based on visual identification, taking also into consideration that tetrads are distorted during fracturing, and platinum deposit varies somewhat between replicas. The sum of particles associated with 4- and 3-particle tetrads is given as a percentage of total particles for each cluster in Table 1, column 2, and the ratio of complete to incomplete tetrads is given in column 3. For RyR1 on the average, 80% of the DHPR particles are components of detectable tetrads, and 4-particle tetrads are 2.5 times as frequent as incomplete ones (Table 1, columns 2 and 3). R4 and R9 give a lower percentage of particles in

TABLE 1 Restoration of tetrads by RyR constructs

RyR/DHPR Isoforms	Max No. of Particles In 3- and 4-Particle tetrads (% of Total, Mean ± SD)	Ratio of 4-Particle/3-Particle Tetrads (mean ± SD)	Avg No. of Particles in Tetrads (% of Total)	Density of Particles No. 10^4 nm^2 (mean ± SD)
a. RyR1/α_{1s}DHPR	80% ± 11% (n = 32)	2.5 ± 1.6	65%	21.0 ± 4.5
b. R9/α_{1s}DHPR	69% ± 13% (n = 31)	2.0 ± 1.7	54%	15.2 ± 4.2
c. R4/α_{1s}DHPR	68% ± 13% (n = 70)	1.2 ± 0.9	47%	21.4 ± 6.2
d. R16/α_{1s}DHPR	55% ± 16% (n = 34)	1.2 ± 1.1	36%	12.3 ± 3.6
e. R10/α_{1s}DHPR	55% ± 11% (n = 24)	1.2 ± 1.0	29%	13.2 ± 5.6
f. RyR2/α_{1s}DHPR	6% ± 9% (n = 52)	—	0.5%	17.9 ± 7.5
g. RyR2/α_{1c}DHPR	7% ± 9% (n = 29)	—	0.7%	19.5 ± 5.5
h. none/α_{1s}DHPR	4% ± 6% (n = 26)	—	0.3%	23.1 ± 8.2

Column 2 gives the average number of particles arranged in 3- and 4-particle tetrads as percentage of the total particles in patches selected for most clearly showing tetrads. The 4- to 3-particle tetrad ratio, column 3, decreases in parallel to the overall frequency of tetrads, while the overall density of particles, column 4, shows no significant trend. The data are arranged in order of decreasing relative frequency of tetrads. As explained in the text, the data were obtained from particle clusters showing at least one tetrad-like arrangement. The number of clusters that have no visible tetrads in transfected cells increases as one progresses down the table, and it jumps to a high value (at least 10-fold) in the last three rows.

Student's *t*-test (column 2). *p* values: g vs. h, 0.2632; f vs h, 0.2153; f vs. g, 0.7237; c vs. a, 0.0003; b vs. a, 0.0006; e vs. b, 0.0002; e vs. c, 0.0004; d vs. b, 0.0001; d vs. c, 0.0005; a vs. f, 0.0001, n = No. of clusters.

tetrads having three to four elements (68% and 69%, respectively) and the difference from RyR1 is statistically highly significant (Student's *t*-test, P values of 0.0003 and 0.0006, respectively). The ratio of 4- to 3-particle tetrads is also lower in R9- and R4- than in RyR1-containing CRUs (2.0 and 1.2 versus 2.5 for RyR1), as expected from visual inspection of the images. Expression of R10 and R16, which gives obvious, even if more disordered, groups of tetrads, resulted in 55% tetrad occupancy, with *p*-values ranging between 0.0001 and 0.0005 relative to R4 and R9, indicating highly significant differences. The ratio of 4- to 3-particle tetrads for both R10 and R16 was 1.2.

RyR1-, R4-, R9-, R16-, and R10-infected cells were compared with 1) control 1B5 cells; 2) RyR2-infected cells; and 3) cardiac myocytes from the finch, samples in which DHPR clusters do not form arrays of tetrads. Occasionally in these samples, particles that are disposed in groups resembling either a 4- or a 3-particle tetrad are seen and we selected clusters that by eye appeared to have at least one such grouping. The data in Table 1, column 2 show that a very low percentage of particles has the specific arrangement typical of a tetrad, even in these selected images, as may be expected if the apparent tetrads originate simply by chance. The 4-/3-particle tetrad ratio could not be calculated for individual DHPR groups in these cells, because each group had 0 content of either one of the other type of tetrad. Complete groups of four are absent in control 1B5 cells, and cardiac myocytes, and in RyR2-expressing 1B5 cells. In parallel to the variation in tetrad occupancy of DHPR clusters, the transfected cells also show variations in the frequency of DHPR clusters that do contain tetrads. An estimate of this variation was obtained by counting the number of DHPR clusters that either contain at least one tetrad, or that have no tetrads. For the transfected cells, the counts were limited to cells that do express RyR. In the case of RyR1, R4, R9, R16, and R10 this was determined by the presence of tetrads; in the case of RyR2 we expected that cells showing clear mounds were expressing the protein (see above). The number of clusters showing tetrads as percentage of total clusters is 81 for RyR2, 78 for R9, 68 for R4, 66 for R16, 53 for R10, 9 for RyR2, 10 for cardiac myocytes, and 8 for control 1B5 cells. Multiplying the data in Table 1, column 2 by the above factors, we obtained an estimate of the average content of particles arranged in tetrads in the DHPR clusters of the various cells (Table 1, column 4). This shows that the tetrads' restoration efficiency is considerably higher for RyR1 and falls gradually for the other constructs in the following sequence: RyR1 R9 R4 R16 R10. These differences do not arise either from variations in the efficiency of targeting of the various constructs to peripheral couplings or to variations in the expression of DHPRs because immunolabeling shows equivalent frequency of RyR foci in all cases (see Fig. 3). Actually, R10- and R16-infected cells consistently show larger numbers of RyR foci than R4.

The formation of complete (or almost complete) tetrads depends on two factors: the DHPRs/RyRs ratio in each patch and the affinity between the two proteins. Because the thin sections usually show feet occupying the whole junctional gap, it is appropriate to assume that a complete array of feet is present beneath the grouped DHPRs; thus the DHPR/RyR ratio is proportional to the DHPR density/area of junctional membrane. The density of DHPR particles in each patch of junctional membrane is given in Table 1, column 5. The DHPR particle density in R4 was approximately the same as for RyR1, so that reduced DHPR expression was not responsible for the slightly lower frequency of tetrad formation in R4 cells. The particle density for R9, R10, and R16 are lower than for RyR1, and this could contribute in part to the reduced frequency of tetrads for R9, R10, and R16.

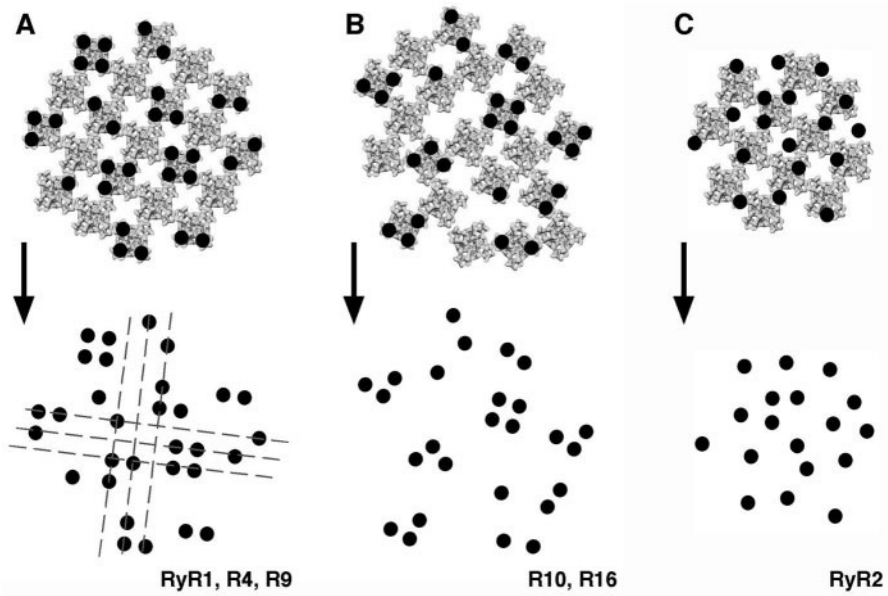

FIGURE 7 Models depicting possible reciprocal arrangements of RyRs and DHPRs within calcium release units of 1B5 cells expressing wild-type and chimeric RyRs. See text for details. At the top of each panel both RyRs (*gray*) and DHPRs (*black*) are represented. At the bottom only DHPRs are shown to mimic what is seen in freeze-fracture replicas. (*A*) Tetrad arrays are quite well-ordered in 1B5 cells expressing RyR1, R4, and R9, suggesting that both chimeras contain in their sequence the RyR region necessary for the physical link with α_{1S}DHPRs. (*B*) R10 and R16 restore tetrads, but the tetrad arrays seem to be less ordered than in cells expressing R4 or R9, because these two chimeras do not form well-organized arrays of feet in the SR membrane. (*C*) RyR2 expression does not restore DHPR tetrads in 1B5 myotubes, but an occasional group of three-tetrad-like particles is seen.

The arrangements of DHPRs in relation to RyR2 and various RyR1-RyR2 chimeras are modeled in Fig. 7. At the top both RyRs (*gray*) and DHPRs (*black*) are represented, while at the bottom only DHPRs are shown, to mimic what is seen in freeze-fracture replicas. In RyR1-, R4-, and R9-expressing 1B5 cells (Fig. 7 *A*), the real images show that DHPRs are located in orthogonal patterns of tetrads. Because a stereospecific association of DHPRs with RyR subunits is necessary for tetrad formation, the disposition of DHPR particles reflects the underlying orthogonal pattern of the RyR (feet) arrays (Fig. 7 *A*, *bottom*, *dashed lines*). Occupancy of alternate feet by complete and incomplete tetrads is quite high. In the diagram of Fig. 7 *B*, representing R10 and R16, the DHPR tetrads (3- and 4-particles) are modeled to have the same stereospecific association with feet as for RyR1. Because in the real images the tetrads are variably oriented, the feet associated with them must also have a variable orientation. The model then extrapolates this variable orientation to all feet and associated particles in the group. It should be noted, however, that particles not forming part of complete tetrads could not be reliably assigned to foot subunits in the case of these two chimeras, because the arrays of feet are partly disjointed. Thus we do not have proof that all (or the majority of) particles are aligned with feet.

RyR2 (Fig. 7 *C*, *top*) is shown to be organized into ordered arrays identical to those for RyR1. In reality, the actual form of RyR2 arrays is not known, despite that fact that feet in cardiac muscle have regular spacings (Fawcett and McNutt, 1969; Junker et al., 1994; Protasi et al., 1996). In the case of RyR2, the specific disposition of feet is not very important in the model. Particles representing α_{1S}-DHPRs are shown not to be stereospecifically associated with RyR2 subunits. The presence of a 3-particle group is extremely rare for RyR2, and it is not clear that it represents an association with RyR2.

Ca^{2+} imaging

Fig. 8 *A* illustrates Ca^{2+} transients recorded from control and RyR-transduced 1B5 cells in response to two sequential stimuli: Ca^{2+}-free 80 mM KCl and 40 mM caffeine (for each construct, the responses of two separate cells are shown). All experiments were performed in nominally Ca^{2+}-free IB, supplemented with 0.5 mM $CdCl_2$ and 0.1 mM $LaCl_3$ to completely block Ca^{2+} currents through DHPRs. A response to caffeine indicates the presence of RyRs in the cell being examined, whereas a response to the Ca^{2+}-free 80 mM K^+ suggests the occurrence of depolarization-induced intracellular Ca^{2+} release that does not rely upon entry of extracellular Ca^{2+} (i.e., skeletal-type e-c coupling). Control cells do not respond to either Ca^{2+}-free 80 mM KCl or 40 mM caffeine, which is expected for cells that do not express RyRs. In all the transduced cultures tested, ~80% of cells (of at least 140 for each group) respond to caffeine (see Table 2), suggesting a very high

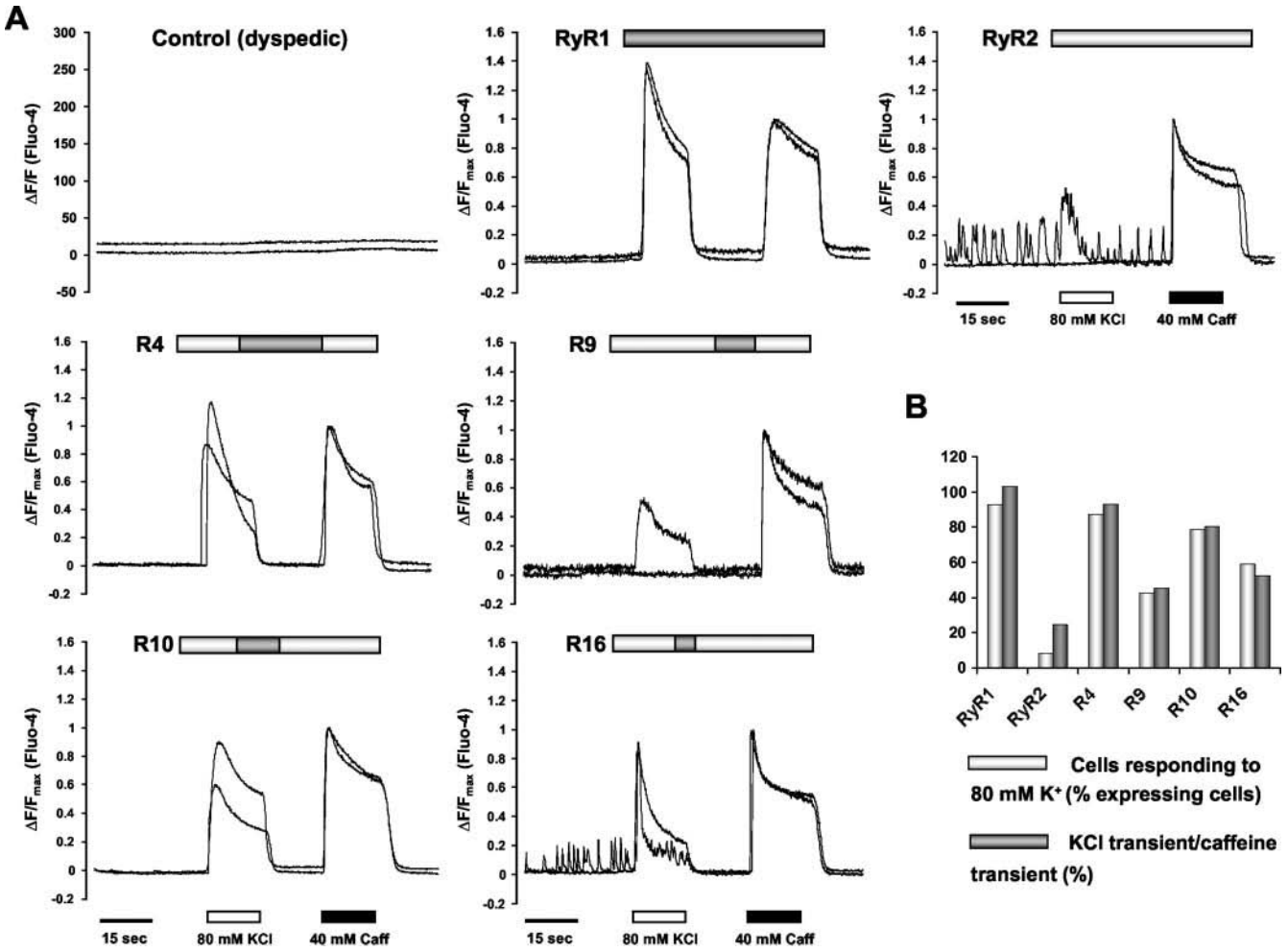

FIGURE 8 (*A*) Response of control and RyR-expressing cells to K^+-induced depolarization and caffeine. All the experiments were performed in nominal Ca^{2+}-free solution containing 0.1 mM La^{3+} and 0.5 mM Cd^{2+} to block Ca^{2+} entry through the DHPR. Data are plotted as $\Delta F/F_{max}$, where F_{max} is the peak amplitude of the transient induced by caffeine (40 mM), and the pre-stimulus fluorescence background has been subtracted. In each panel traces from two simultaneously imaged cells are shown superimposed. Control cells did not respond either to K^+ or to caffeine. In transduced cells, responses to Ca^{2+}-free 80 mM KCl and to caffeine were restored, but the relative magnitude of the responses varied with the construct. RyR1-expressing cells responded to Ca^{2+}-free 80 mM KCl with a Ca^{2+} transient often larger than the caffeine one. RyR2 expressing cells gave very small Ca^{2+} transients in response to Ca^{2+}-free 80 mM KCl in very few cells (<10%), but a robust caffeine response. Various chimeras showed an intermediate behavior: R4 gave the largest responses, followed by R10 and R16, with R9 giving the smallest responses. Note that in the experiments illustrated for RyR2 and R9, only one of the two cells responded to Ca^{2+}-free 80 mM KCl and that one of each of the cells expressing RyR2 and R16 showed spontaneous activity. Quantitative analysis of functional experiments is reported in Table 2. (*B*) Comparison of intracellular Ca^{2+} responses of wild-type and chimeric RyRs. *Light gray bars:* percentage of RyR-expressing cells (i.e., cells responding to caffeine) that respond to Ca^{2+}-free 80 mM KCl (data from Table 2). *Dark gray bars:* magnitude of the Ca^{2+}-free 80 mM KCl transient as a percentage of the caffeine transient in the same cell (see Methods). RyR1 gave both the highest fraction of cells responding to Ca^{2+}-free 80 mM KCl and the largest amount of Ca^{2+} released, while RyR2 had the lowest values for both parameters. The chimeric RyRs gave intermediate results in the order: R4 > R10 > R16 > R9.

efficiency of transfection/expression. Of those cells that produce caffeine transients, a variable fraction also produces a transient in response to Ca^{2+}-free 80 mM KCl. The fraction of cells that respond to depolarization, and the normalized peak amplitude of this depolarization-response, were taken as the two criteria of the ability of each construct to mediate skeletal-type e-c coupling (Fig. 8 *B*). The depolarization-response is normalized by the caffeine-response as a way of correcting for possible variations in level of RyR expression, relative volume of junctional SR, extent of SR Ca^{2+} loading, and loading of the indicator dye (Fluo-4). In many cases the magnitude of K^+-induced transients is larger than that of the subsequent caffeine response, especially in RyR1- and R4-expressing myotubes. Because K^+ depolarization elicits large transients in RyR1- and R4-expressing cells, and because the caffeine challenge occurs only 15 s after the K^+ depolarization, it seemed possible that the SR may have been partially depleted before the application of caffeine. To test this possibility, we performed identical experiments on primary myotubes from

TABLE 2 Restoration of skeletal-type e-c coupling by RyR constructs

RyR/DHPR Isoforms	No. Cells Imaged	% Imaged Cells Responding to 40 mM Caffeine	% Imaged Cells Responding to 80 mM K^+, 0 Ca^{2+}	% 80 mM K^+, 0 Ca^{2+}/40 mM Caffeine Responses
RyR1/α_{1s}DHPR	201	75.6	70.1	92.8
R4/α_{1s}DHPR	140	78.6	68.6	87.3
R10/α_{1s}DHPR	144	78.5	61.8	78.8
R16/α_{1s}DHPR	136	83.8	49.3	58.8
R9/α_{1s}DHPR	276	81.1	34.4	42.4
RyR2/α_{1s}DHPR	208	75.9	6.2	8.2
none/α_{1s}DHPR	164	none	none	none

Note that for each construct a large number of myotubes was imaged (minimum of 136) and that in each sample group ~80% of cells responded to caffeine, consistent with the immunostaining results of Fig. 2, suggesting a high efficiency of viral transduction. Note also that the fraction of cells responding to K^+ varies considerably between constructs. The data in column 4 are plotted as a bar graph in Fig. 8 *B* (*light gray bars*).

wild-type mice (results not shown) that express more constant amounts of both α_{1S}DHPR and RyR1. In these experiments we observed that regardless of the order in which the two pulses were applied (K^+ first or caffeine first), the response to K^+ was always larger than the response to caffeine. This result suggests that 80 mM K^+ depolarization is more effective than 40 mM caffeine as a Ca^{2+}-releasing stimulus.

RyR1 is the most effective construct at restoring skeletal-type e-c coupling: a large fraction of RyR1-expressing cells respond to depolarization, giving a normalized response of large amplitude (Fig. 8 *B* and Table 2). By contrast, a small fraction of RyR2-expressing cells respond to Ca^{2+}-free 80 mM KCl, and the normalized amplitude of the response is much smaller. Among the chimeras, R4 is the most effective in restoring Ca^{2+} release induced by Ca^{2+}-free 80 mM KCl, both in number of cells responding and in the magnitude of the transient. R10, R16, and R9 follow this in order of decreasing effectiveness. However, even R9 gives much more frequent and larger responses to Ca^{2+}-free 80 mM KCl than did RyR2 (Fig. 8 *B* and Table 2). Overall, Fig. 8 *B* shows a striking correspondence between the frequency of cells that were capable of a response to the Ca^{2+}-free K^+-challenge and the normalized magnitude of the Ca^{2+} transient. Based on these data, the constructs can be ordered based on their efficiency in restoring skeletal-type e-c coupling: RyR1 > R4 > R10 ≫ R16 > R9 ≫ RyR2. Note that in addition to releasing Ca^{2+} in response to stimulation, the transduced cells also produce spontaneous Ca^{2+} transients. This occurs very rarely in RyR1-expressing cells and very frequently in RyR2-expressing cells, with the chimeras showing intermediate behaviors. In Fig. 8 *A*, spontaneous activity is clearly visible in one of the traces in the RyR2 and R16 panels.

DISCUSSION

In the present study we have analyzed freeze-fracture replicas and intracellular Ca^{2+} transients of 1B5 myotubes expressing various RyR constructs, with the goal of comparing the ability of these constructs to restore skeletal-type e-c coupling and their ability to organize α_{1S}DHPRs into junctional tetrads. The constructs examined were the skeletal-RyR1, the cardiac-RyR2, and the chimeric RyR1/RyR2 constructs R4 (Sk: 1635–3720), R9 (Sk: 2659–3720), R10 (Sk: 1635–2559), and R16 (Sk: 1837–2154). Based on immunostaining, thin-section electron microscopy, and response to caffeine all of these proteins were expressed at similar levels, targeted to junctions between the SR and plasma membrane and functional as Ca^{2+} release channels. With respect to their ability to organize α_{1S}DHPRs into tetrads, they ranked in decreasing effectiveness as RyR1 > R4 = R9 > R10 = R16 ≫ RyR2. As judged by Ca^{2+} transients elicited by K^+ depolarization in a Ca^{2+}-free external medium, the rank order for restoration of skeletal-type e-c coupling was RyR1 > R4 > R10 > R16 > R9 ≫ RyR2.

The method we used to test for skeletal e-c coupling (15 s in a Ca^{2+}-free medium containing Cd^{2+} and La^{3+}) made it possible to measure internal Ca^{2+} releases of varying magnitudes in large numbers of cells and thus to obtain a rank-order of the ability of the various RyR constructs to restore skeletal-type e-c coupling (Fig. 8 *B* and Table 2). Several of these RyR constructs have also been examined in previous physiological studies. In one study, Nakai et al. (1998a) applied 10 ms electrical stimuli to Fluo-3 AM-loaded myotubes in a Ca^{2+}-free medium and found that RyR1-, R4-, and R10-expressing cells produced similar Ca^{2+} transients (indicative of skeletal e-c coupling), whereas R9 and RyR2 failed to produce transients. More recently, Proenza et al. (2002) found that 10-ms stimuli caused 10/13 intact myotubes expressing RyR1 to contract in a Ca^{2+}-free medium, whereas 3/30 expressing R16 contracted, and 0/30 expressing RyR2 contracted. Thus, these previous results are consistent with a rank-order of RyR1/R4/R10 > R9/RyR2 (Nakai et al., 1998a) and RyR1 > R16 > RyR2 (Proenza et al., 2002), which is generally in agreement with the rank-order found for skeletal e-c coupling in our present work (Fig. 8 *B*). However, unlike the present work, the earlier studies failed to produce evidence for skeletal-type coupling for R9 or RyR2. Most likely, the much longer depolarizations used in the present work (15 s)

made it possible to detect releases too small to be detected in response to the briefer stimuli (10 ms). In addition, in the present work we used HSV1 virions to transduce 1B5 myotubes. This system delivers cDNA into muscle cells much more efficiently and gives a much higher expression level than the mono-nuclear injection of primary myotubes (Wang et al., 2000; Fessenden et al., 2000; Protasi et al., 2000). It is also important to note that spatially averaged measurements of myoplasmic free Ca^{2+} are only an indirect assay of RyR activation, which means that different assays can give different quantitative estimates of the relative ability of different RyRs to mediate e-c coupling. For example, the data of Fig. 8 *B* indicate that R16 is about half as effective as RyR1 in mediating skeletal e-c coupling. By contrast, the average value of peak Ca^{2+} transients in R16-expressing myotubes was found to be only ~14% of that in RyR1-expressing cells when measured with 200-ms depolarizations applied via whole patch clamping (Proenza et al., 2002). Whether or not this is actually a better estimate, it emphasizes that while the data of Fig. 8 *B* are important for providing a rank ordering, they cannot be taken as a linear comparison between constructs.

Of the chimeras examined, R4 (which contains the most RyR1 sequence) is closest to RyR1 in ability to restore skeletal e-c coupling (Fig. 8 *B*). Moreover, the function of R4 can be partially carried out by subregions within its amino-terminal half (R10 and the shorter segment, R16). The carboxyl-terminal half of R4 (contained in R9 and not in R10 or R16) also rescues e-c coupling, although less effectively than either the R10 or R16 segments. Thus, we conclude that skeletal e-c coupling depends on a functional interaction between α_{1S}DHPR and RyR1, which involves at least two separate regions of RyR1, and that the full functional interaction results from additive effects of two or possibly more regions. A similar conclusion was also reached in an earlier study of R16 and its complementary construct, "R16-reverse" (Proenza et al., 2002).

As mentioned earlier, signaling between the α_{1S}DHPR and RyR1 is bidirectional: in addition to e-c coupling (orthograde signaling), there is also retrograde signaling that increases the magnitude of Ca^{2+} current carried via the α_{1S}DHPR (Nakai et al., 1996). Based on measurements of Ca^{2+} current density in dyspedic myotubes expressing RyR constructs (Nakai et al., 1998a; Proenza et al., 2002), the rank-order for retrograde signaling is RyR1 > R4 = R9 > R10 ≫ R16, that is, very similar to their ability to organize α_{1S}DHPRs into tetrads. Thus, the rank-orders of R9 and R10 in orthograde signaling and retrograde signaling/tetrad restoration are opposite. The bidirectional signaling between α_{1S}DHPR and RyR1 strongly suggests a mechanical interaction between the two proteins, and it is difficult to imagine how such a mechanical interaction could occur without physical linkages. In this regard, the occurrence of tetrads is very important because it is indicative of a stereospecific DHPR/RyR association that, in turn, implies physical linkages. We observed tetrads for all those RyR constructs that were more effective in restoring skeletal e-c coupling. The different constructs showed a slightly different rank-order for the restoration of tetrads (Table 1) than for the restoration of skeletal e-c coupling (Fig. 8 *B* and Table 2). In particular, the subdomain of R4 that is most effective in forming tetrads (the one contained in R9) is not the segment that is most effective in restoring skeletal type e-c coupling (the one contained in R10 or R16). Although this lack of correlation might appear to be at odds with the notion that e-c coupling requires physical linkages, it should be recalled that the signaling between RyR1 and α_{1S}DHPR is bidirectional, and that for retrograde signaling R9 appears to be more effective than R10. Furthermore, one would suppose that the interaction between the α_{1S}DHPR and a chimeric RyR responsible for e-c coupling would depend on the presence of two features: 1) one or more sites of the chimeric RyR that participates in physical linkage to the α_{1S}DHPR, and 2) structures within the RyR that couple mechanical alteration of the linkage site to opening of the Ca^{2+} release channel. A chimera could contain regions that participate in physically linking to the DHPR but lack all or part of the appropriate structures for the intermolecular conformational changes (within the RyR) which convert α_{1S}DHPR conformational changes to RyR channel opening. According to this reasoning, it is not necessarily surprising that a chimera unable to mediate effective e-c coupling could nonetheless be effective at organizing DHPRs into tetrads. However, the hypothesis that e-c coupling depends on mechanical interactions would be called seriously into question if one were to find an RyR construct that was functionally equivalent to, but that lacked the ability to, organize DHPRs into tetrads. That was not the case in our results.

As for functional rescue by the RyR chimeras, the structural rescue of tetrads appears to depend upon two separate regions of RyR1. Both the R4 region and its carboxyl-terminal half, R9, are sufficient to produced organized arrays of DHPR tetrads. However, the amino-terminal half of R4 also appears to be involved to some extent in the physical interaction, because both R10 and its R16 subdomain are able to restore tetrads to a lesser degree (Table 1). Although the entire R4 region represents a substantial amount of primary sequence, folding of this region might produce a single pocket that physically links to the DHPR. Fig. 9 illustrates a hypothetical model of how the folded RyR might interact with the α_{1S}DHPR II-III loop. Of course, neither the functional nor the freeze-fracture data provide any evidence as to whether the physical linkage between α_{1S}DHPR and RyR1 is direct or involves other proteins. A recent report by O'Reilly et al. (2002) suggests a role of FKBP12 in the interaction between the II-III loop and RyR1. However, yeast two-hybrid analysis demonstrates a direct in vitro interaction between the R16 region of RyR1 and a 46-residue segment of the α_{1S}DHPR II-III

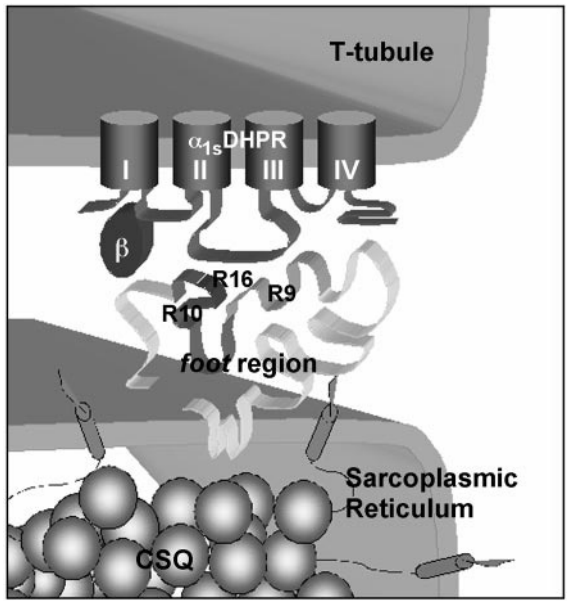

FIGURE 9 Model suggesting how noncontiguous regions of RyR1 could fold to interact with the α_{1S}DHPR. The chimeras examined in this study contain RyR1 regions that are all part of the foot region of the protein according to the folding models of both Takeshima et al. (1989) and Zorzato et al. (1990). The R4 region, shown in three gradations of gray, is illustrated as interacting with the II-III loop of the α_{1S}DHPR, which has been shown to be critical for skeletal-type e-c coupling (Tanabe et al., 1990; Grabner et al., 1999; Wilkens et al., 2001). Within R4, R10 (1635–2636, *medium gray*) and its R16 subdomain (1837–2154, *dark gray*) are much more effective in carrying out skeletal e-c coupling than is R9 (2659–3720, *lighter gray*); the latter region is shown as having a greater region of contact with the II-III loop because R9 is more effective at organizing DHPRs into tetrad arrays. However, our data cannot exclude the possibility that domains of the α_{1S}DHPR other than the II-III loop, or of RyR1 outside of the R4 region, are involved in "mechanical" coupling.

loop (Proenza et al., 2002), consistent with the idea that these two regions contact one another in vivo. Interestingly, a somewhat weaker interaction was also observed between the II-III loop segment and the portion of RyR2 that corresponds to the R16 region of RyR1 (Proenza et al., 2002). If this interaction can also occur in vivo, it might help to explain the very weak functional and structural coupling that we observed between RyR2 and α_{1S}DHPR.

We thank S. Murkejee, R. Hirsh, Y. Wang, T. Yang, and N. Glaser for technical support. We thank Drs. T. Wagenknecht and M. Samso for providing us with RyR cryomicroscopy reconstruction images that have been used in Fig. 7. We also thank Dr. G. Meissner for his generous gift of C3-33 antibodies. The 34C monoclonal antibody developed by J. A. Airey and J. Sutko (Airey et al., 1990) was obtained from the Developmental Studies Hybridoma Bank developed under the auspices of the NICHD and maintained by the University of Iowa, Dept. of Biological Sciences, Iowa City, IA 52242.

This work was supported by National Institutes of Health Grant AR PO144650 (to P.D.A., K.G.B., and C.F.-A.) and by Grant MDA 2688 (to P.D.A. and F.P.).

REFERENCES

Adams, B. A., T. Tanabe, A. Mikami, S. Numa, and K. G. Beam. 1990. Intramembrane charge movement restored in dysgenic skeletal muscle by injection of dihydropyridine receptor cDNAs. *Nature (Lond.).* 346: 569–572.

Airey, J. A., C. F. Beck, K. Murakami, S. J. Tanksley, T. J. Deerinck, M. Ellisman, and J. L. Sutko. 1990. Identification and localization of two triad junction foot protein isoforms in mature avian fast twitch skeletal muscle. *J. Biol. Chem.* 265:14187–14194.

Avila, G., and R. T. Dirksen. 2000. Functional impact of the ryanodine receptor on the skeletal muscle L-type Ca^{2+} channel. *J. Gen. Physiol.* 115:467–480.

Beam, K. G., C. M. Knudson, and J. A. Powell. 1986. A lethal mutation in mice eliminates the slow calcium current in skeletal muscle cells. *Nature.* 320:168–170.

Block, B. A., T. Imagawa, K. P. Campbell, and C. Franzini-Armstrong. 1988. Structural evidence for direct interaction between the molecular components of the transverse tubule/sarcoplasmic reticulum junction in skeletal muscle. *J. Cell Biol.* 107:2587–2600.

Buck, E. D., A. H. Nguyen, I. N. Pessah, and P. D. Allen. 1997. Dyspedic mouse skeletal muscle expresses major elements of the triadic junction but lacks ryanodine receptor protein and function. *J. Biol. Chem.* 272: 7360–7367.

Chaudhari, N. 1992. A single nucleotide deletion in the skeletal muscle-specific calcium channel transcript of muscular dysgenesis (mdg) mice. *J. Biol. Chem.* 267:25636–25639.

Cohen, S. A., and D. W. Pumplin. 1979. Clusters of intramembranous particles associated with binding sites for alpha-bungarotoxin in cultured chick myotubes. *J. Cell Biol.* 82:494–516.

Coronado, R., J. Morrissette, M. Sukhareva, and D. M. Vaughan. 1994. Structure and function of ryanodine receptors. *Am. J. Physiol. Cell Physiol.* 266:C1485–C1491.

Fabiato, A. 1983. Calcium-induced release of calcium from cardiac sarcoplasmic reticulum. *Am. J. Physiol. Cell Physiol.* 245:C1–C14.

Fabiato, A. 1985. Simulated calcium current can both cause calcium loading in and trigger calcium release from the sarcoplasmic reticulum of a skinned canine cardiac Purkinje cell. *J. Gen. Physiol.* 85:291–320.

Fawcett, D. W., and N. S. McNutt. 1969. The ultrastructure of the cat myocardium. I. Ventricular papillary muscle. *J. Cell Biol.* 42:1–45.

Ferguson, D. G., H. Schwartz, and C. Franzini-Armstrong. 1984. Subunit structure of junctional feet in triads of skeletal muscle. A freeze-drying, rotary-shadowing study. *J. Cell Biol.* 99:1735–1742.

Fessenden, J. D., Y. Wang, R. A. Moore, S. R. W. Chen, P. D. Allen, and I. N. Pessah. 2000. Divergent physiological and pharmacological properties of ryanodine receptor type 1 and 3 expressed in a myogenic cell line. *Biophys. J.* 79:2509–2525.

Fosset, M., E. Jaimovich, E. Delpont, and M. Lazdunski. 1983. [^{3}H]nitrendipine receptors in skeletal muscle. *J. Biol. Chem.* 258:6086–6092.

Fraefel, C., S. Song, F. Lim, P. Lang, L. Yu, Y. Wang, P. Wild, and A. I. Geller. 1996. Helper virus-free transfer of HSV-1 plasmid vectors into neuronal cells. *J. Virology.* 70:7190–7197.

Franzini-Armstrong, C. 1984. Freeze-fracture of frog slow-tonic fibers. Structure of surface and internal membranes. *Tissue Cell.* 16:647–664.

Franzini-Armstrong, C., and J. W. Kish. 1995. Alternate disposition of tetrads in peripheral couplings of skeletal muscle. *J. Muscle Res. Cell Motil.* 16:319–324.

Franzini-Armstrong, C., and F. Protasi. 1997. The ryanodine receptor of striated muscles, a complex capable of multiple interactions. *Physiol. Rev.* 77:699–729.

Franzini-Armstrong, C., F. Protasi, and V. Ramesh. 1999. Shapes, sizes and distributions of Ca^{2+} release units and couplons in a variety of skeletal and cardiac muscles. *Biophys. J.* 77:1528–1539.

Grabner, M., R. T. Dirksen, N. Suda, and K. G. Beam. 1999. The II-III loop of the skeletal muscle dihydropyridine receptor is responsible for the bi-directional coupling with the ryanodine receptor. *J. Biol. Chem.* 274:21913–21919.

Junker, J., J. R. Sommer, M. Sar, and G. Meissner. 1994. Extended junctional sarcoplasmic reticulum of avian cardiac muscle contains functional ryanodine receptors. *J. Biol. Chem.* 269:1627–1634.

Meissner, G. 1994. Ryanodine receptor/Ca^{2+} release channels and their regulation by endogenous effectors. *Annu. Rev. Physiol.* 56:485–508.

Moore, R. A., H. Nguyen, J. Galceran, I. N. Pessah, and P. D. Allen. 1998. A transgenic myogenic cell line lacking ryanodine receptor protein for homologous expression studies: reconstitution of Ry_1R protein and function. *J. Cell Biol.* 140:843–851.

Nakai, J., R. T. Dirksen, H. T. Nguyen, I. N. Pessah, K. G. Beam, and P. D. Allen. 1996. Enhanced dihydropyridine receptor channel activity in the presence of ryanodine receptor. *Nature (Lond.).* 380:72–75.

Nakai, J., T. Ogura, F. Protasi, C. Franzini-Armstrong, P. D. Allen, and K. G. Beam. 1997. Functional non-equality of the cardiac and skeletal ryanodine receptors. *Proc. Natl. Acad. Sci. U.S.A.* 94:1019–1022.

Nakai, J., N. Sekiguchi, T. A. Rando, P. D. Allen, and K. G. Beam. 1998a. Two regions of the ryanodine receptor involved in coupling with L-type Ca^{2+} channels. *J. Biol. Chem.* 273:13403–13406.

Nakai, J., T. Tanabe, T. Konno, B. A. Adams, and K. G. Beam. 1998b. Localization in the II-III loop of the dihydropyridine receptor of a sequence critical for excitation-contraction coupling. *J. Biol. Chem.* 273:24983–24985.

O'Reilly, F. M., M. Robert, I. Jona, C. Szegedi, M. Albrieux, S. M. Geib, M. De Waard, M. Villaz, and M. Ronjat. 2002. FKBP12 modulation of the binding of the skeletal ryanodine receptor onto the II-III loop of the dihydropyridine receptor. *Biophys. J.* 82:145–155.

Osame, M., A. G. Engel, C. J. Rebouche, and R. E. Scott. 1981. Freeze-fracture electron microscopic analysis of plasma membranes of cultured muscle cells in Duchenne dystrophy. *Neurology.* 31:972–979.

Pincon-Raymond, M., F. Rieger, M. Fosset, and M. Lazdunski. 1985. Abnormal transverse tubule system and abnormal amount of receptors for Ca^{2+} channel inhibitors of the dihydropyridine family in skeletal muscle from mice with embryonic muscular dysgenesis. *Nature (Lond.).* 325:717–720.

Proenza, C., J. J. O'Brien, J. Nakai, S. Mukherjee, P. D. Allen, and K. G. Beam. 2002. Identification of a region of RyR1 that participates in allosteric coupling with the α_{1S} ($Ca_V1.1$) II-III loop. *J. Biol. Chem.* 277:6530–6535.

Protasi, F., C. Franzini-Armstrong, and P. D. Allen. 1998. Role of the ryanodine receptors in the assembly of calcium release units in skeletal muscle. *J. Cell Biol.* 140:831–842.

Protasi, F., C. Franzini-Armstrong, and B. E. Flucher. 1997. Coordinated incorporation of skeletal muscle dihydropyridine receptors and ryanodine receptors in peripheral couplings of BC_3H1 cells. *J. Cell Biol.* 137:859–870.

Protasi, F., X-H. Sun, and C. Franzini-Armstrong. 1996. Formation and maturation of calcium release apparatus in developing and adult avian myocardium. *Dev. Biol.* 173:265–278.

Protasi, F., H. Takekura, Y. Wang, S. R. Chen, G. Meissner, P. D. Allen, and C. Franzini-Armstrong. 2000. RYR1 and RYR3 have different roles in the assembly of calcium release units of skeletal muscle. *Biophys. J.* 79:2494–2508.

Rios, E., and G. Brum. 1987. Involvement of dihydropyridine receptors in excitation-contraction coupling in skeletal muscle. *Nature (Lond.).* 325: 717–720.

Rios, E., J. Ma, and A. Gonzales. 1991. The mechanical hypothesis of excitation-contraction coupling in skeletal muscle. *J. Muscle Res. Cell Motil.* 12:127–129.

Schneider, M. F. 1994. Control of calcium release in functioning skeletal muscle fibers. *Annu. Rev. Physiol.* 56:463–484.

Schneider, M. F., and W. K. Chandler. 1973. Voltage dependence charge movement in skeletal muscle: a possible step in excitation contraction coupling. *Nature (Lond.).* 242:244–246.

Sutko, J. L., and J. A. Airey. 1996. Ryanodine receptor Ca^{2+} release channel: does diversity in form equal diversity in function? *Phys. Rev.* 76:1027–1071.

Takekura, H., and C. Franzini-Armstrong. 1999. Correct targeting of dihydropyridine receptors and triadin in dyspedic mouse skeletal muscle in vivo. *Dev. Dyn.* 214:372–380.

Takekura, H., M. Nishi, T. Noda, H. Takeshima, and C. Franzini-Armstrong. 1995. Abnormal junctions between surface membrane and sarcoplasmic reticulum in skeletal muscle with a mutation targeted to the ryanodine receptor. *Proc. Natl. Acad. Sci. U.S.A.* 92:3381–3385.

Takeshima, H., M. Iino, H. Takekura, M. Nishi, J. Kuno, O. Minowa, H. Takano, and T. Noda. 1994. Excitation-contraction uncoupling and muscular degeneration in mice lacking functional skeletal muscle ryanodine-receptor gene. *Nature (Lond.).* 369:556–559.

Takeshima, H., N. Nishimura, T. Matsumoto, H. Ishida, K. Kangawa, N. Minamino, H. Matsuo, M. Ueda, M. Hanaoka, T. Hirose, and S. Numa. 1989. Primary structure and expression from complementary DNA of skeletal muscle ryanodine receptor. *Nature (Lond.).* 339:439–445.

Tanabe, T., K. G. Beam, B. A. Adams, T. Niidome, and S. Numa. 1990. Regions of the skeletal muscle dihydropyridine receptor critical for excitation-contraction coupling. *Nature.* 344:451–453.

Tanabe, T., K. G. Beam, J. A. Powell, and S. Numa. 1988. Restoration of excitation-contraction coupling and slow calcium current in dysgenic muscle by dihydropyridine receptor complementary DNA. *Nature (Lond.).* 336:134–139.

Tanabe, T., H. Takeshima, A. Mikami, V. Flockerzi, H. Takahashi, K. Kangawa, M. Kojioma, H. Matsuo, T. Hirose, and S. Numa. 1987. Primary structure of the receptor for calcium channel blockers from skeletal muscle. *Nature (Lond.).* 328:313–318.

Wang, Y., C. Fraefel, F. Protasi, R. A. Moore, J. D. Fessenden, I. N. Pessah, A. DiFrancesco, X. Breakefield, and P. D. Allen. 2000. HSV-1 amplicon vectors are a highly efficient gene delivery system for skeletal muscle myoblasts and myotubes. *Am. J. Physiol. Cell Physiol.* 47: C619–C623.

Wilkens, C. M., N. Kasielke, B. E. Flucher, K. G. Beam, and M. Grabner. 2001. Excitation-contraction coupling is unaffected by drastic alteration of the sequence surrounding residues L720–L764 of the alpha 1S II-III loop. *Proc. Natl. Acad. Sci. U.S.A.* 98:5892–5897.

Zorzato, F., J. Fujii, K. Otsu, M. Phillips, N. M. Green, F. A. Lai, G. Meissner, and D. H. MacLennan. 1990. Molecular cloning of cDNA encoding human and rabbit forms of the Ca^{2+} release channel (ryanodine receptor) of skeletal muscle sarcoplasmic reticulum. *J. Biol. Chem.* 265:2244–2256.